Deposition of TiO_2 Nanoparticles onto Silica Measured Using a Quartz Crystal Microbalance with Dissipation Monitoring

Revised and resubmitted to:

Langmuir

March 22, 2009

JULIEN FATISSON[1], RUTE F. DOMINGOS[2], KEVIN J. WILKINSON[2], and NATHALIE TUFENKJI[*,1]

[1]*Department of Chemical Engineering, McGill University, Montreal, Quebec H3A 2B2, Canada*

[2]*Department of Chemistry, University of Montreal Montreal, Quebec H3C 3J7, Canada*

[*] Corresponding Author. Phone: (514) 398-2999; Fax: (514) 398-6678; E-mail: nathalie.tufenkji@mcgill.ca

Abstract

Titanium dioxide (TiO_2) nanoparticles introduced into subsurface environments may lead to contamination of drinking water supplies and can act as colloidal carriers for sorbed contaminants. A model laboratory system was used to examine the influence of water chemistry on the physicochemical properties of TiO_2 and their deposition. Deposition rates of TiO_2 particles onto a silica surface were measured over a broad range of solution conditions (pH and ionic strength) using a quartz crystal microbalance with energy dissipation monitoring (QCM-D). Higher particle deposition rates were observed under favorable interaction conditions (i.e., in the presence of attractive electrostatic interactions) in comparison to unfavorable deposition conditions where electrostatic repulsion dominated particle-surface interactions. Nanoparticle sizes were characterized by fluorescence correlation spectroscopy (FCS), dynamic light scattering (DLS), and atomic force microscopy (AFM). These analyses confirmed the nanoscale of the system under study as well as the presence of TiO_2 aggregates in some cases. TiO_2 deposition behavior onto silica measured using QCM-D was generally found to be in qualitative agreement with the Derjaguin-Landau-Verwey-Overbeek (DLVO) theory of colloidal stability.

Keywords: *Titanium dioxide nanoparticles, quartz crystal microbalance, dissipation factor, DLVO, fluorescence correlation spectroscopy, zeta potential.*

1. Introduction

The global market for nanotechnology was evaluated at $USD 9.4 billion in 2005 and is expected to increase to $1 trillion by 2015[1]. Indeed, an increasing number of nanosized components are being incorporated into commercial products for performance enhancement. Engineered materials such as nanoparticles, nanorods and nanotubes play a role in a wide range of domains including electronics, biomedical applications, cosmetics, pharmaceuticals, and energy. Although engineered nanomaterials hold great promise due to their unique physicochemical properties, little is known about their transport and fate in the natural environment nor their potential cytotoxicity[2].

The Organization for Economics Cooperation and Development (OECD) recently placed TiO_2 on its priority list of representative manufactured nanomaterials that require in-depth characterization (http://www.olis.oecd.org). TiO_2 is widely used in different commercial products, such as paints, sunscreens, and pigments. Although preliminary research reported by Wiesner and Bottero[1] demonstrates the ecotoxicity of TiO_2, the environmental fate and behavior of this nanomaterial has not been well characterized. A few studies have examined the transport and retention of TiO_2 nanoparticles in an effort to understand the contamination potential of this material in the natural subsurface environment[3-6]. Laboratory column and micromodel studies have been used to investigate the migration potential of TiO_2 nanoparticles in model granular porous media representative of the natural subsurface[3-6]. This research showed that TiO_2 transport depended on solution pH[4] and flow velocity in some cases[3, 6], as observed for several other colloids or biocolloids in aqueous environments[7-9]. Recently, in an extensive study of the aggregation behavior of TiO_2 nanoparticles[10], TiO_2 aggregation was shown to be most important at high solution ionic strengths

and pHs close to its pH_{zpc}. Although some researchers have characterized the physicochemical properties and transport behavior of TiO_2 nanoparticles in granular porous media, our understanding of the deposition behavior of this material over a range of environmentally relevant conditions is incomplete.

In addition to the traditional laboratory column experiments, the quartz crystal microbalance (QCM) has recently been shown to be an effective technique to monitor the attachment of molecules, particles, viruses or cells onto clean or functionalized surfaces[11-18]. Although the QCM-D has been widely used to measure the adsorption kinetics of macromolecules such as proteins[19, 20], few researchers have used this technique to monitor the deposition kinetics of nanoparticles[11, 12, 15, 16, 18]. Chen and Elimelech[11, 12] used a QCM-D to examine the deposition kinetics of carbon-based (fullerene) nanoparticles in the presence of monovalent and divalent salts. In their work, the mass of nanoparticles deposited on a silica surface was related to the measured decrease in the resonance frequency of a QCM-D crystal. Quevedo and Tufenkji used a similar approach to quantify the deposition kinetics of a CdTe quantum dot over a broad range of water chemistries[18]. Another approach to characterize particle or cell deposition/attachment using the QCM-D is the measurement of the energy dissipation factor, D[21].

The purpose of this study is to examine the deposition rates of TiO_2 nanoparticles onto model sand (SiO_2) surfaces. The QCM-D was used to measure anatase TiO_2 deposition onto clean silica by following changes in the resonance frequency (f) and the energy dissipation factor (D) over a broad range of environmentally relevant solution chemistries, including variations in ionic strength, pH and ion valence. The particle deposition behavior is related to variations in particle charge (evaluated using

measurements of electrophoretic mobility) and particle size (determined by dynamic light scattering, DLS, and fluorescence correlation spectroscopy, FCS).

2. Materials and Methods

2.1. Preparation of Nanoparticle Suspensions

A stock suspension of TiO_2 (1 g/L) was prepared by suspending TiO_2 powder (reported diameter: 5 nm, NanoAmor, USA) in deionized (DI) water. TiO_2 suspensions (10 mg/L) were prepared by diluting the stock suspension into a number of $NaNO_3$ (Sigma-Aldrich) solutions prepared at different salt concentrations (I=1–100 mM) at pH 3.0±0.1. The suspension prepared at 10 mg/L (pH 3) was kept at 4 °C overnight, then vigorously shaken using a vortex mixer set at high speed, and finally the pH was adjusted to 5 or 9 using 0.05 M NaOH (Fisher) one hour prior to each experiment. The suspensions were gently mixed one additional time before conducting the experiments. All chemicals used to prepare solutions were of analytical grade.

2.2. Nanoparticle Sizing

Dynamic light scattering (Malvern ZetaSizer Nano) and fluorescence correlation spectroscopy (Leica TCS SP5 laser scanning microscope using ISS Vista ISS FCS software, version 3.6) were used to measure the hydrodynamic diameters of the TiO_2. For FCS measurements, the TiO_2 particles were labeled using 10^{-8} M rhodamine 6G (Sigma-Aldrich), which corresponds to <0.1% surface coverage of the fluorophore. An optimized setting of 30 to 120 sec was used for the acquisitions, with 15 repetitions. Excitation of the fluorophore was accomplished using an Ar ion laser at 514 nm,

corresponding to the maximum excitation wavelength for this rhodamine derivative. All FCS measurements were performed at 22±1 °C. Diffusion times were determined by calibrating the dimensions of the confocal volume using rhodamine 110 which has a known diffusion coefficient of 4.4×10^{-10} m^2 s^{-1} in water[22]. Weight average diffusion coefficients were determined from the measured diffusion times across the calibrated confocal volume. DLS and FCS measurements were conducted using at least three independent samples.

2.3. Nanoparticle Imaging

Atomic force microscopy (AFM) and transmission electron microscopy (TEM) was also employed to confirm the TiO_2 particle size distribution under selected conditions. For the AFM observations, TiO_2 suspensions were pipetted onto mica surfaces and left to sit for 4 hrs (Veeco Instruments Inc., NY) to allow particle deposition. The mica was air dried and analyzed in tapping mode with standard silicon nitride cantilevers (Nanoworld, USA). At least 20 images were taken of each particle covered mica sheet at a resolution of 256 × 256 pixels using a scan frequency of 1 Hz. AFM images were analyzed to determine individual particle sizes using image processing software (Image J)[23]. Size distributions were determined from height measurements of a minimum of 140 particles from at least 20 independent AFM images of a single particle covered mica sheet. Transmission electron microscopy (TEM) was also used to obtain higher resolution images of the TiO_2 particles under selected conditions. In this case, samples were prepared by placing a drop of the TiO_2 suspension on a formvar grid, which was left to air dry overnight prior to analysis. Measurements were performed

on a Philips CM200 microscope equipped with an AMT CCD camera and operating at 200 kV with a LaB_6 filament.

2.4. Electrokinetic Characterization of TiO_2 particles.

Laser Doppler velocimetry (ZetaSizer Nano ZS, Malvern) was used to characterize the electrophoretic mobility (EPM) of the nanoparticles in $NaNO_3$. Samples were briefly centrifuged to remove large aggregates (6,200×*g*, 1 min). EPM measurements were repeated using at least three different samples (prepared on different days) at 20.0±0.2 °C. The strength of the applied electrical field (*E*) was 4.9±0.1V. Measured EPMs were converted to ζ-potential using the Smoluchowski equation[24].

2.5. Quartz crystal microbalance with dissipation (QCM-D) measurements.

QCM-D measurements were performed with a Q-Sense E4 unit (Q-Sense AB, Göteborg, Sweden) by simultaneously monitoring the changes in frequency (Δf) and energy dissipation (ΔD) of a 5 MHz silica coated QCM-D crystal (QSX-303). The QCM-D crystal is excited to oscillate in the thickness-shear mode at its fundamental resonance frequency (f_0=5 MHz), at odd overtones (n = 3, 5, or 7) by applying a radio-frequency voltage across the electrodes. Energy dissipation of the crystal is periodically recorded by measuring the exponentially dissipated sinusoidal voltage signal over the crystal caused by switching off the voltage applied to the piezoelectric oscillator. The Q-Sense software (QSoft) was then used to acquire the *D* factor via equation 1:

$$D = \frac{E_{\text{dissipated}}}{2\pi E_{\text{stored}}} \quad (1)$$

where $E_{dissipated}$ is the energy lost during one oscillation cycle and E_{stored} is the total energy stored in the oscillator. The D factor provides information on the deposition process as well as on some of the viscoelastic properties of the deposited layer. In the case of homogeneous, very thin or quasi-rigid layers, the frequency shift of the oscillating crystal (Δf) can be related to the increase in mass per unit area, Δm_f, by the Sauerbrey[25] relationship:

$$-\Delta f = \frac{1}{nC}\Delta m_f \qquad (2)$$

where the mass sensitivity constant, C, is equal to 17.7 ng.cm^{-2} Hz^{-1} when f = 5 MHz. Prior to each experiment, the silica coated quartz crystals were cleaned in a UV-ozone chamber for 10 min. The crystals were then mounted in four separate QCM-D flow chambers, stabilized at 20.00 ± 0.02°C, with only one side in contact with the working solution. A background $NaNO_3$ electrolyte at the pH and ionic strength of interest was injected at 0.40 mL/min until a stable baseline was reached. Subsequently, a suspension of TiO_2 particles in the same electrolyte was injected into the flow chambers (0.40 mL/min) for 20 min. Finally, the background electrolyte solution was injected at the same flow rate for a final 20 min. Frequency and dissipation shifts were continuously recorded during the entire experiment. QCM-D experiments were repeated using at least three different samples (prepared on different days). After each experiment, the crystals, chambers and tubing were rinsed with 5 mL of 2% sodium dodecyl sulfate (SDS) (Sigma-Aldrich), 20 mL of DI, 5 mL of 2% Hellmanex (Fisher) and 30 mL of DI. Because the dissipation factor (D) is a ratio of energies (Eq. 1), it is dimensionless and is reported as 10^{-6} dissipation units (DU).

3. Results and Discussion

3.1. Characterization of TiO_2.

3.1.1. Sizing analysis

Particle size can play a critical role in the transport potential and environmental fate of colloids in aquatic systems[26-28]. Moreover, it has been shown that the suspension preparation method can significantly influence the size and aggregation of TiO_2[29]. Hence, it is important to characterize the size of the particles used in this study in order to better understand the influence of solution chemistry on TiO_2 particle size and deposition behavior.

The nominal TiO_2 particle diameter reported by the manufacturer is 5 nm. Even after transformation to number average diameters, DLS measurements revealed particle sizes on the order of 350 to 750 nm (Figure 1a) depending on ionic strength and pH. Measured hydrodynamic diameters generally increased with increasing $NaNO_3$ concentration at each pH. The particles appeared smaller at pH 3 in comparison to the higher pHs. Because the scattering intensity of the particles is roughly proportional to d^6 (Rayleigh approximation), DLS measurements are strongly influenced and highly sensitive to the presence of aggregates. Another investigation conducted under similar conditions has also reported the presence of TiO_2 aggregates using DLS[30].

[FIGURE 1 HERE]

Particle polydispersity has much less of an influence on hydrodynamic diameters determined by FCS[31] as compared to diameters determined by DLS. Indeed, FCS determined weight averaged particle diameters were in the range of 7 to 189 nm (Fig. 1b). Nonetheless, a similar trend of increasing

particle size was observed with increasing salt concentration. No significant differences were observed between results acquired at pH 3 and pH 9, however particle sizes at pH 5 were noticeably larger. Note that the FCS technique is somewhat limited for larger particles because the confocal volume can only accomodate a particle on the order of 200 nm in size.

As a third independent evaluation of particle diameter, AFM images were acquired for TiO_2 suspensions prepared for different solution chemistries (e.g. Fig. 1c, 2 mM $NaNO_3$, pH 3). Height measurements of at least 140 particles were accumulated to produce particle size distributions (e.g. Fig. 1d, 2 mM $NaNO_3$, pH 3). A large fraction of the TiO_2 particles had sizes below 50 nm with a smaller number of particles being observed in the larger size domains. Similar results were obtained for other solution conditions with average observed particle sizes of approximately 30 nm for all observations at pH 3 (10, 30 and 100 mM $NaNO_3$). Overall, particle sizes determined by AFM were in good agreement with FCS measurements, but suggest that the suspensions could not simply be described by a single particle size. In another study, Choy et al[3] also observed the simultaneous presence of TiO_2 aggregates and single particles in their study performed at pH 4.5, I = 10 mM.

TEM imaging carried out on selected samples confirmed the small nanometer sizes of the TiO_2 suspensions (Figure S1). By combining all of the sizing techniques, it appears that the TiO_2 sample studied is mostly composed of very small particles (~ 30 nm) and a smaller number of aggregates between 100 and 500 nm in size and that more aggregates were present at pH 5. As mentioned above, the aggregates, even when present in small quantities, can create significant bias in the DLS measurements. FCS, AFM and TEM analysis confirmed the presence of a large proportion of nanoparticles in the suspensions studied.

3.1.2 Electrophoretic mobility (EPM) measurements

Electrophoretic mobility measurements made for a large range of solution chemistries were converted to ζ-potentials (Figure 2). In the presence of the monovalent salt, at pH 3 and 5, the particles were positively charged while they were negative at pH 9, in accordance with previous studies conducted using anatase nanoparticles[32, 33]. Indeed, the measured EPM was near zero at pH 5, which is close to the pH_{zpc} previously reported for nanosized anatase (5.8[34] and 5.1[35]). In a related study, the EPM of the same TiO_2 product (from NanoAmor) was evaluated over a range of pHs and the pH_{zpc} was found to be in the range of 4.5 to 5.2[10]. At the lowest and highest pH values, absolute ζ-potentials decreased with increasing ionic strength of the sodium salt, consistent with an increased charge screening. The ζ-potential and size data reported in Figure 1b and 2a are used later in the paper to interpret the results obtained by QCM-D within the context of DLVO theory.

[FIGURE 2 HERE]

3.2. TiO_2 deposition kinetics on clean silica.

3.2.1. Frequency and dissipation signals during TiO_2 deposition onto silica

Figure 3a shows representative QCM-D measurements following injection of a TiO_2 suspension at pH 3 in 10 mM $NaNO_3$ electrolyte. These conditions correspond to favorable conditions for deposition where attractive electrostatic interactions dominate the interaction between the particles and the silica surface. Following injection of the TiO_2 suspension into the QCM-D module, a decrease

in frequency and an increase in dissipation are observed (Phase 1), resulting from nanoparticle deposition onto the silica surface. During phase II, a particle-free solution of $NaNO_3$ at the same I and pH is injected into the flow module resulting in a stabilization in the frequency and dissipation shifts during this period (i.e., there is no change in attached mass at the crystal surface).

[FIGURE 3 HERE]

Because the frequency shift (Δf) is proportional to a change in mass (Δm) at the crystal surface (Eq. 2), the rate of change of Δf is equivalent to the rate of mass change on the crystal surface (i.e., the rate of particle deposition or release). Hence, the TiO_2 deposition rate can be determined by calculating the initial slope in the Δf plot (e.g., phase I in Figure 3a). The dissipation factor (D) also provides an indication of the mass attached to the crystal surface but also takes into account the "viscoelasticity" of the attached particle layer. The addition of a perfectly rigid mass to the crystal surface will yield zero additional D. However, the deposition of each particle onto the crystal surface can add a similar amount of energy loss which is reflected in D. Thus, the variation in ΔD with time can also be used as a means to evaluate the particle deposition rate (e.g., from the slope of the light grey curve in phase I of Figure 3a). To better understand how solution chemistry (pH and I) influences the TiO_2 deposition rate, the slopes of the frequency shift (f_{slope}) and the dissipation shift (D_{slope}) were calculated from the data obtained during the initial portion of phase I (e.g., Fig. 4). Comparison of Fig. 4a and 4b shows that the error bars obtained for at least 3 replicate measurements were generally wider in the case of the calculated f_{slope} than for the calculated D_{slope} (particularly at low I). This behavior has been reported previously[36] and indicates that, in some cases, the measurement of

dissipation (D) can be a more reliable parameter than the measurement of resonance frequency. For example, Poitras and Tufenkji[21] also demonstrated that the shift in dissipation was a more sensitive response signal than the frequency shift for detection of the bacterium *E. coli* O157:H7. Thus, for the sake of simplicity, the D_{slope} has been chosen as the parameter of interest in the discussion that follows. However it is important to note that the trends in f_{slope} are very similar to those observed for D_{slope}.

[FIGURE 4 HERE]

3.2.2. Effect of pH and ionic strength on TiO_2 deposition

Higher values of D_{slope} (and larger absolute values of f_{slope}) are indicative of higher TiO_2 deposition rates. Inspection of Figure 4b reveals higher values of D_{slope} under conditions where attractive electrostatic forces predominate; namely, when the surface is negatively charged and the particles are positively charged (at pH 3 and 5). At pH 3 and 5, D_{slope} decreases with increasing I, indicating lower TiO_2 deposition rates on the silica surface. As the ionic strength increases, the diffuse double-layer is compressed, surface charges are screened and consequently, the electrostatic attraction between the particle and surface is attenuated. This behavior is in qualitative agreement with DLVO theory (also see below) and several other studies examining colloidal deposition or aggregation under favorable conditions[37, 38]. Furthermore, at a given ionic strength, lower TiO_2 deposition rates were observed at pH 5 as compared to pH 3. In this case, the nanoparticles are less positive at pH 5 than at pH 3 (Figure 2a) and exhibit considerably more aggregation at pH 5 (Figure 1). Dunphy Guzman

et al[4] also reported variations in TiO_2 deposition with changes in pH. These trends will be explained in more detail within the context of DLVO theory later in the paper.

When repulsive electrostatic interactions dominate the particle-surface interaction (i.e., particles and silica surface are both negatively charged at pH 9), the TiO_2 deposition rate (i.e., D_{slope}) is near zero at low I. This observation can be explained by the fact that at low I, the particle charge is not effectively screened and hence the electrostatic repulsion between the TiO_2 and the silica surface is strong. This behavior is consistent with a number of other studies examining particle or microbe deposition[7, 9, 39-41]. As I increases, both particle and surface charges are more effectively screened as the thickness of the diffuse double-layer decreases. Because repulsive forces are reduced, increased TiO_2 deposition results. This is demonstrated by the increase of D_{slope} with I at pH 9 (Figure 4b). It is interesting to note that the f_{slope} at pH 9 was very low over the range of I and in some cases, the values of f_{slope} were positive (Figure 4a). A positive value of f_{slope} is associated with a positive frequency shift. This behavior may be attributed to the formation of thick viscoelastic films on the crystal surface, or an apparently high viscosity at the liquid-crystal interface resulting from accumulation of weakly attached particles. Hence, the observed positive f_{slope} at pH 9 is consistent with the presence of electrostatic repulsive forces that can be expected when the silica surface and the TiO_2 particles are similarly charged.

At high I (i.e., above 100 mM), the rate of TiO_2 deposition represented by the D_{slope} is similar (around 0.05 DU/min) for all examined pHs (Fig. 4). As discussed, at high I ($I \geq 60$ mM), all charges are screened to the point that no significant differences can be observed between the particle deposition

rates. Indeed, careful inspection of Figure 2a reveals that for all three pH values, ζ–potential values are approaching zero at the highest *I*.

For the system examined in this study, it is not straightforward to evaluate the mass of particles deposited on the silica surface from the raw QCM-D data. Difficulties arise in converting the measured *f* shifts to units of mass due to the inherent heterogeneity of the particle population (i.e., polydispersity) and the relatively high measured *D* shifts. The Sauerbrey relation (Eq. 2) is considered inappropriate for inhomogeneous films and likely underestimates the deposited mass in the system examined here. Nonetheless, if the Sauerbrey relationship was valid for this type of system, calculations show that the measured *f* shifts correspond to deposition rates of a few ng per min (Table S1, Supporting Information).

3.2.3. Effect of ion valence on TiO_2 deposition

The influence of ion valence on TiO_2 ζ-potential and deposition kinetics was investigated by replacing the sodium salt ($NaNO_3$) with a calcium salt, $Ca(NO_3)_2$ for experiments run at pH 3 and 9 (Figs. 2b and 5). The trends in the ζ-potentials in the presence of the divalent salt were similar to those observed in the presence of $NaNO_3$. At pH 3, the particles were positively charged while they were negative at the lower ionic strengths at pH 9 and became near-neutrally charged at the highest ionic strengths at pH 9 (Fig. 2b). Experiments conducted at pH 3 with calcium nitrate showed a similar trend to those using sodium nitrate (Fig. 5, open squares). At low ionic strength, the TiO_2 deposition rate is highest and in the same range as that observed with $NaNO_3$. As the salt concentration increased, the value of D_{slope}, and, correspondingly the particle deposition rate, decreased.

[FIGURE 5 HERE]

Experiments conducted at pH 9 in the presence of the calcium salt revealed no significant difference in the TiO_2 deposition rate over the range of *I* examined (Fig. 5, open triangles). The particle deposition rate at this pH is close to the maximum obtained with $NaNO_3$ at pH 9; ~ 0.05 DU/min (Fig. 5, solid triangles).

3.3. DLVO interpretation of TiO_2 deposition kinetics.

To better understand the mechanisms controlling the observed TiO_2 deposition behavior, DLVO theory was used to calculate colloidal interaction energies. DLVO theory considers the sum of London-van der Waals (VDW) and electrical double-layer (EDL) interactions. The total interaction energy, namely, the sum of VDW and EDL interactions, was determined by treating the particle-silica system as a sphere-plate interaction. Constant-potential EDL interactions were calculated using the expression of Hogg *et al.*[42], where the ζ-potentials of the TiO_2 particles and the silica surface were used in place of the respective surface potentials. TiO_2 ζ-potentials were taken from Figure 2a, whereas silica ζ-potentials were taken from Bergna and Roberts[43] or extrapolated from the data of Walker *et al.*[44]. The retarded VDW attractive interaction energy was calculated from the expression proposed by Gregory[45]. A value of 1×10^{-20} J was chosen for the Hamaker constant for the silica-water-TiO_2 system[46]. Nanoparticle sizes were taken from values obtained from the FCS measurements (Figure 6a-c) or from the DLS measurements (Figure 6d-f) (Table S2).

[FIGURE 6 HERE]

DLVO interaction energy profiles for the TiO_2-silica system in the presence of a monovalent salt are presented in Figure 6. At pH 3 (Figure 6a,d), no energy barrier is present such that DLVO calculations predict completely favorable conditions for deposition of the positively charged particles onto the negatively charged silica surface. At this pH, the energy well forms at a larger particle-surface separation at 2 mM as compared to the higher ionic strengths. These calculations suggest that for a TiO_2 particle approaching a silica surface, the attractive interaction will be felt at greater separation distances at an ionic strength of 2 mM as opposed to 100 mM. The calculated interaction energy profiles are consistent with the observed deposition rates for TiO_2 (i.e. 2 mM >10 mM >100 mM; Figure 4). Indeed, Elimelech and Song[37, 47] used theoretical calculations to show that attractive double layer interactions can extend to larger distances at lower *I*, thereby enhancing particle deposition.

At pH 5, the trends in the DLVO profiles are not in as good agreement with the deposition behavior when the particle size determined by FCS is used (Figure 4 and Figure 6b); namely, the starting point of the energy well is not always located at greater separation distances at lower *I*. Also, the decay in the interaction energy profile appears slightly steeper at pH 5 (Figure S2) than at pH 3, although greater particle deposition rates were noted at pH 3 in comparison to pH 5. It is important to note that the pH_{zpc} of TiO_2 is very near pH 5, and this is indeed the pH at which we observed important aggregation (Figure 2b). Indeed, aggregation is likely occurring over the time scale of the deposition experiments at this pH. The formation of aggregates can lead to decreased deposition due to decreased convective-diffusive transport to the silica surface as well as a decrease in the effective particle number concentration. Hence, the poorer agreement between DLVO calculations and QCM

measurements at pH 5 may be attributed to the instability of the TiO_2 suspension at this pH. Nonetheless, the DLVO calculations determined using the particle size based on DLS (Figure 6e) are in good qualitative agreement with the particle deposition behavior.

At pH 9, the particles and the silica surface are both negatively charged, and hence, unfavorable conditions for deposition predominate (Figure 6c,f). The DLVO calculations presented in Figure 6c,f suggest that at ionic strengths of 2 mM and 10 mM, the repulsive energy barrier will effectively prevent TiO_2 particles from depositing on the silica surface. Such a result is consistent with QCM-D measurements that revealed little or no particle deposition at pH 9 at the low ionic strengths (Figure 4). On the other hand, when the salt concentration is increased to 100 mM, the repulsive energy barrier is eliminated (Figure 6c,f), and the conditions become more favorable for particle deposition, in agreement with measured values of D_{slope}. At the high ionic strengths, observations of similar deposition rates at each of the pH values (Figure 4) are explained by the fact that at 100 mM, the DLVO interaction energy profiles are very similar for all three pH values (Figure S2c,f). In general, the DLVO calculations based on the two different sets of measured particle sizes (FCS versus DLS) are in good agreement, except at pH 5 where we note slight disagreement at the higher *I*. To our knowledge, this is the first attempt to characterize TiO_2 nanoparticle-silica interactions over a wide range of solution chemistries using DLVO theory. Although DLVO theory is useful for providing insight into the mechanisms controlling the particle deposition behavior, it is important to note the limitations of comparing the experimental QCM-D results to DLVO theory; for instance, the theory assumes the interaction of perfectly spherical, uniformly-sized particles with a flat and homogeneous collector surface.

3.4. Monitoring TiO_2 detachment using QCM-D.

To better understand the risk of TiO_2 particle release from sand surfaces in aqueous environments, selected detachment experiments were also conducted using the QCM-D. For example, particle release from a surface can occur following specific changes in solution chemistry[4, 28, 48] as a result of rainfall or due to surface water-groundwater exchange. In Figure 3a, TiO_2 particles were deposited in 10 mM $NaNO_3$ at pH 3 (phase I), followed by an injection of particle-free electrolyte at the same *I* and pH (phase II). During phase II of this favorable deposition experiment, there is no detectable change in the *f* or *D* shifts, indicative of no release of particles from the silica surface. In phase III, a particle-free solution of $NaNO_3$ at higher *I* (100 mM) and identical pH is injected into the flow module. Even though the solution chemistry has been changed in phase III leading to changes in the particle and surface ζ-potential, there was no observable effect on the deposited particles. Because the particles deposited in phase I were deposited under completely favorable conditions, they are believed to be trapped in the primary energy well of the DLVO interaction energy profile (Figure 6a, d).

On the other hand, the strong interaction between the TiO_2 particles and the silica surface can be disrupted by a particle-free solution at higher pH and very low ionic strength (10 mM NaOH; pH 12) injected into the flow module (Fig. 3a, phase IV). In this case, a rapid increase in frequency and a corresponding decrease in dissipation were observed during this phase of the experiment. At pH 12, both the particles and the silica surface are negatively charged such that the attractive interactions are replaced with strong repulsive electrostatic interactions.

Particles were generally released more readily when they were deposited under conditions deemed unfavorable (i.e., when repulsive electrostatic interactions predominate)[49]. When TiO_2 particles were deposited at pH 9 and 100 mM $NaNO_3$, detachment of the particles was observed during phase III when ionic strength was decreased to 10 mM (pH 9) (Fig. 3b). Similar behavior has been observed when examining the deposition behavior of fullerene aggregates using QCM-D[11]; namely, the presence of repulsive interactions were sufficient to weaken attachment and led to particle detachment. This result is also in agreement with previous studies of particle deposition under unfavorable conditions[49, 50] which demonstrate that when the surface and particles are similarly charged, the deposition of particles is reversible and weaker than that observed when electrostatic interactions are attractive.

4. Conclusions

This study reports for the first time TiO_2 nanoparticle-silica interactions over a broad range of environmentally relevant solution pHs and ionic strengths. The slope in the dissipation shift (D_{slope}) from QCM-D measurements is shown to be a useful indicator of particle deposition behavior. Water chemistry was shown to play a significant role on the TiO_2 deposition rate. Under favorable conditions for deposition (i.e., pH 3 and 5), the maximum deposition rate was observed at low ionic strength as a result of strong attractive electrostatic interactions between the nanoparticles and the surface. Increasing ionic strength led to a decrease in deposition rate when the particles and the surface were oppositely charged. The contrary was observed under unfavorable conditions, where the particles and the silica surface are similarly charged. Under these conditions, low deposition rates were measured at

low ionic strength with particle deposition increasing at higher salt concentrations. In general, TiO_2 deposition kinetics, determined by measurements of the frequency and dissipation slopes, were in good qualitative agreement with classical DLVO theory at pH 3 and 9. This study also reports for the first time a comprehensive analysis of TiO_2 nanoparticle size using several complementary experimental techniques (DLS, AFM, FCS, and TEM) over a wide range of water chemistries. The results also highlight the limitations of DLS in characterizing polydisperse suspensions.

Acknowledgements

This work is supported by the Natural Sciences and Engineering Research Council of Canada (NSERC Strategic Grant no. 350638), the Fonds québécois de la recherche sur la nature et les technologies (FQRNT), and the Canada Research Chairs (CRC) program.

References

1. Wiesner, M. R.; Bottero, J.-Y., *Environmental Nanotechonology: Applications and Impacts of Nanomaterials*. The McGraw-Hill Companies: 2007; p 540.
2. Nowack, B.; Bucheli, T. D. *Environmental Pollution* **2007,** *150* (1), 5-22.
3. Choy, C. C.; Wazne, M.; Meng, X. *Chemosphere* **2008,** *71* (9), 1794-1801.
4. Dunphy Guzman, K. A.; Finnegan, M. P.; Banfield, J. F. *Environmental Science & Technology* **2006,** *40* (24), 7688-7693.
5. Lecoanet, H. F.; Bottero, J.-Y.; Wiesner, M. R. *Environmental Science and Technology* **2004,** *38* (19), 5164-5169.
6. Lecoanet, H. F.; Wiesner, M. R. *Environmental Science and Technology* **2004,** *38* (16), 4377-4382.
7. Li, X.; Johnson, W. P. *Environmental Science & Technology* **2005,** *39*, 1658-1665.
8. Abudalo, R. A.; Bogatsu, Y. G.; Ryan, J. N.; Harvey, R. W.; Metge, D. W.; Elimelech, M. *Environmental Science & Technology* **2005,** *39*, 6412-6419.
9. Ryan, J. N.; Elimelech, M. *Colloids and Surfaces, A: Physicochemical and Engineering Aspects* **1996,** *107*, 1-56.
10. Domingos, R. F.; Tufenkji, N.; Wilkinson, K. J. *Environmental Science and Technology* **2009,** *43* (5), 1282-1286.
11. Chen, K. L.; Elimelech, M. *Langmuir* **2006,** *22* (26), 10994-11001.
12. Chen, K. L.; Elimelech, M. *Environmental Science & Technology* **2008,** *42* (20), 7607-7614.
13. Fatisson, J.; Merhi, Y.; Tabrizian, M. *Langmuir* **2008,** *24* (7), 3294-3299.
14. Lord, M. S.; Modin, C.; Foss, M.; Duch, M.; Simmons, A.; Pedersen, F. S.; Besenbacher, F.; Milthorpe, B. K. *Biomaterials* **2008,** *29* (17), 2581-2587.
15. Saleh, N.; Sirk, K.; Liu, Y.; Phenrat, T.; Dufour, B.; Matyjaszewski, K.; Tilton, R. D.; Lowry, G. V. *Environmental Engineering Science* **2007,** *24* (1), 45-57.
16. Stalgren, J. J. R.; Claesson, P. M.; Warnheim, T. *Advances in Colloid and Interface Science* **2001,** *89-90*, 383-394.
17. Steinmetz, N. F.; Bock, E.; Richter, R. P.; Spatz, J. P.; Lomonossoff, G. P.; Evans, D. J. *Biomacromolecules* **2008,** *9* (2), 456-462.
18. Quevedo, I. R.; Tufenkji, N. *Environmental Science & Technology* **2009**, in press.
19. Hook, F.; Voros, J.; Rodahl, M.; Kurrat, R.; Boni, P.; Ramsden, J. J.; Textor, M.; Spencer, N. D.; Tengvall, P.; Gold, J.; Kasemo, B. *Colloids and Surfaces, B: Biointerfaces* **2002,** *24* (2), 155-170.
20. Zhou, A.; Muthuswamy, J. *Sensors and Actuators, B: Chemical* **2004,** *B101* (1-2), 8-19.
21. Poitras, C.; Tufenkji, N. *Biosens Bioelectron* **2009,** *24*, 2137-2142.
22. Avaltroni, F.; Seijo, M.; Ulrich, S.; Stoll, S.; Wilkinson, K. J. *Biomacromolecules* **2007,** *8* (1), 106-112.
23. Balnois, E.; Papastavrou, G.; Wilkinson, K. J. *IUPAC Series on Analytical and Physical Chemistry of Environmental Systems* **2007,** *10* (Environmental Colloids and Particles Behaviour, Separation and Characterisation), 405-467.
24. Hunter, R. J., *Foundations of Colloid Science, 2nd Edition*. 2001; p 806 pp.
25. Sauerbrey, G. *Zeitschrift fuer Physik* **1959,** *155*, 206-22.
26. Litton, G. M.; Olson, T. M. *Colloids and Surfaces, A: Physicochemical and Engineering Aspects* **1996,** *107*, 273-83.
27. Pelley, A. J.; Tufenkji, N. *Journal of Colloid and Interface Science* **2008,** *321* (1), 74-83.
28. Tufenkji, N.; Elimelech, M. *Environmental Science and Technology* **2004,** *38* (2), 529-536.
29. Chen, X.; Mao Samuel, S. *Chemical reviews* **2007,** *107* (7), 2891-959.
30. Pettibone, J. M.; Cwiertny, D. M.; Scherer, M.; Grassian, V. H. *Langmuir* **2008,** *24* (13), 6659-6667.

31. Starchev, K.; Buffle, J.; Perez, E. *Journal of Colloid and Interface Science* **1999,** *213* (2), 479-487.
32. Gustafsson, J.; Mikkola, P.; Jokinen, M.; Rosenholm, J. B. *Colloids and Surfaces, A: Physicochemical and Engineering Aspects* **2000,** *175* (3), 349-359.
33. Ridley, M. K.; Hackley, V. A.; Machesky, M. L. *Langmuir* **2006,** *22* (26), 10972-10982.
34. Pena, M.; Meng, X.; Korfiatis, G. P.; Jing, C. *Environmental Science and Technology* **2006,** *40* (4), 1257-1262.
35. Kormann, C.; Bahnemann, D. W.; Hoffmann, M. R. *Journal of Physical Chemistry* **1988,** *92* (18), 5196-201.
36. Fredriksson, C.; Khilman, S.; Kasemo, B.; Steel, D. M. *Journal of Materials Science: Materials in Medicine* **1998,** *9* (12), 785-788.
37. Elimelech, M.; Song, L. *Separations Technology* **1992,** *2* (1), 2-12.
38. Elimelech, M. *Journal of Colloid and Interface Science* **1991,** *146* (2), 337-52.
39. Tufenkji, N.; Elimelech, M. *Langmuir* **2005,** *21* (3), 841-852.
40. Tufenkji, N. *Water Resources Research* **2006,** *42* (12), W12S11.
41. Johnson, W. P.; Li, X.; Assemi, S. *Advances in Water Resources* **2007,** *30*, 1432-1454.
42. Hogg, R.; Healy, T. W.; Fuerstenau, D. W. *Transactions of the Faraday Society* **1966,** *62* (6), 1638-51.
43. Bergna, H. E.; Roberts, W. O.; Editors, *Colloidal Silica: Fundamentals and Applications. [In: Surfactant Sci. Ser.; 2006, 131]*. 2006; p 912 pp.
44. Walker, S. L.; Bhattacharjee, S.; Hoek, E. M. V.; Elimelech, M. *Langmuir* **2002,** *18* (6), 2193-2198.
45. Gregory, J. *Journal of Colloid and Interface Science* **1981,** *83* (1), 138-45.
46. Feiler, A.; Jenkins, P.; Ralston, J. *Physical Chemistry Chemical Physics* **2000,** *2* (24), 5678-5683.
47. Elimelech, M. *Separations Technology* **1994,** *4* (4), 186-212.
48. Franchi, A.; O'Melia, C. R. *Environmental Science and Technology* **2003,** *37* (6), 1122-1129.
49. Hahn, M. W.; Abadzic, D.; O'Melia, C. R. *Environmental Science and Technology* **2004,** *38* (22), 5915-5924.
50. Tufenkji, N.; Elimelech, M. *Langmuir* **2004,** *20*, 10818-10828.

Figure Captions

Figure 1. Measured TiO_2 particle size determined using several techniques: (a) DLS measurements of TiO_2 suspensions over a range of IS ($NaNO_3$) at pH 3 (■), pH 5 (▲) and pH 9 (▼); (b) FCS measurements over a range of IS ($NaNO_3$), at pH 3 (■), pH 5 (▲) and pH 9 (▼); (c) AFM height mode image of TiO_2 nanoparticles deposited onto mica from a 10 mg/L solution in 2 mM $NaNO_3$ at pH 3; (d) Particle distribution obtained from analysis of 30 AFM height mode images for a 10 mg/L TiO_2 suspension deposited onto mica in 2 mM $NaNO_3$ at pH 3. Data represent the mean ± 95% confidence interval.

Figure 2. Calculated ζ-potentials from electrophoretic mobility measurements of TiO_2 particles over a range of I in (a) $NaNO_3$ at pH 3 (■), pH 5 (▲) and pH 9 (▼); and (b) $Ca(NO_3)_2$ at pH 3 (□) and pH 9 (▽). Data represent the mean ± 95% confidence interval.

Figure 3. Representative QCM-D measurements (frequency and dissipation shifts, 3rd overtone) for deposition of TiO_2 onto SiO_2 coated QCM-D crystals. (a) Phase I: injection of TiO_2 particles suspended in 10 mM $NaNO_3$ at pH 3, Phase II: injection of 10 mM $NaNO_3$ at pH 3, Phase III: injection of 100 mM $NaNO_3$ at pH 3, and Phase IV: injection of 10 mM NaOH (pH 12). (b) Phase I: injection of TiO_2 particles suspended in 100 mM $NaNO_3$ at pH 9, Phase II: injection of 100 mM $NaNO_3$ at pH 9, Phase III: injection of 10 mM $NaNO_3$ at pH 9, and Phase IV: injection of 10 mM NaOH (pH 12). Baseline corrections have been made to take into account shifts in f and D resulting solely from changes in solution chemistry (i.e., in the absence of particles).

Figure 4. Average measured values of (a) f_{slope} and (b) D_{slope} determined from the 3rd overtone measurements during deposition of TiO_2 onto silica at different solution conditions: pH 3 (■ and solid line), pH 5 (▲ and dashed line), and pH 9 (▼ and dotted line). Data represent the mean ± 95% confidence interval.

Figure 5. Average measured values of (a) f_{slope} and (b) D_{slope} (from 3rd overtone measurements) determined during deposition of TiO_2 suspended in a divalent salt ($Ca(NO_3)_2$) as a function of I at different pH: pH 3 (□ and solid line) and pH 9 (▽ and dotted line). D_{slope} values from Figure 4 obtained at pH 9 (▼) have been added in (b) for direct comparison between monovalent and divalent salts. Data represent the mean ± 95% confidence interval.

Figure 6. Calculated DLVO interaction energy profiles for a TiO_2 nanoparticle approaching a flat SiO_2 surface at (a) pH 3, (b) pH 5, and (c) pH 9 for different I ($NaNO_3$): 2 mM (solid lines), 10 mM (dotted lines) and 100 mM (dashed lines). Nanoparticle sizes were taken from values obtained from the FCS measurements (Fig. 1b) and are listed in Table S2. Calculated DLVO interaction energy profiles for a TiO_2 particle approaching a flat SiO_2 surface at (d) pH 3, (e) pH 5, and (f) pH 9 for different I ($NaNO_3$) using sizes obtained from the DLS measurements (Fig. 1a) as listed in Table S2.

Figures

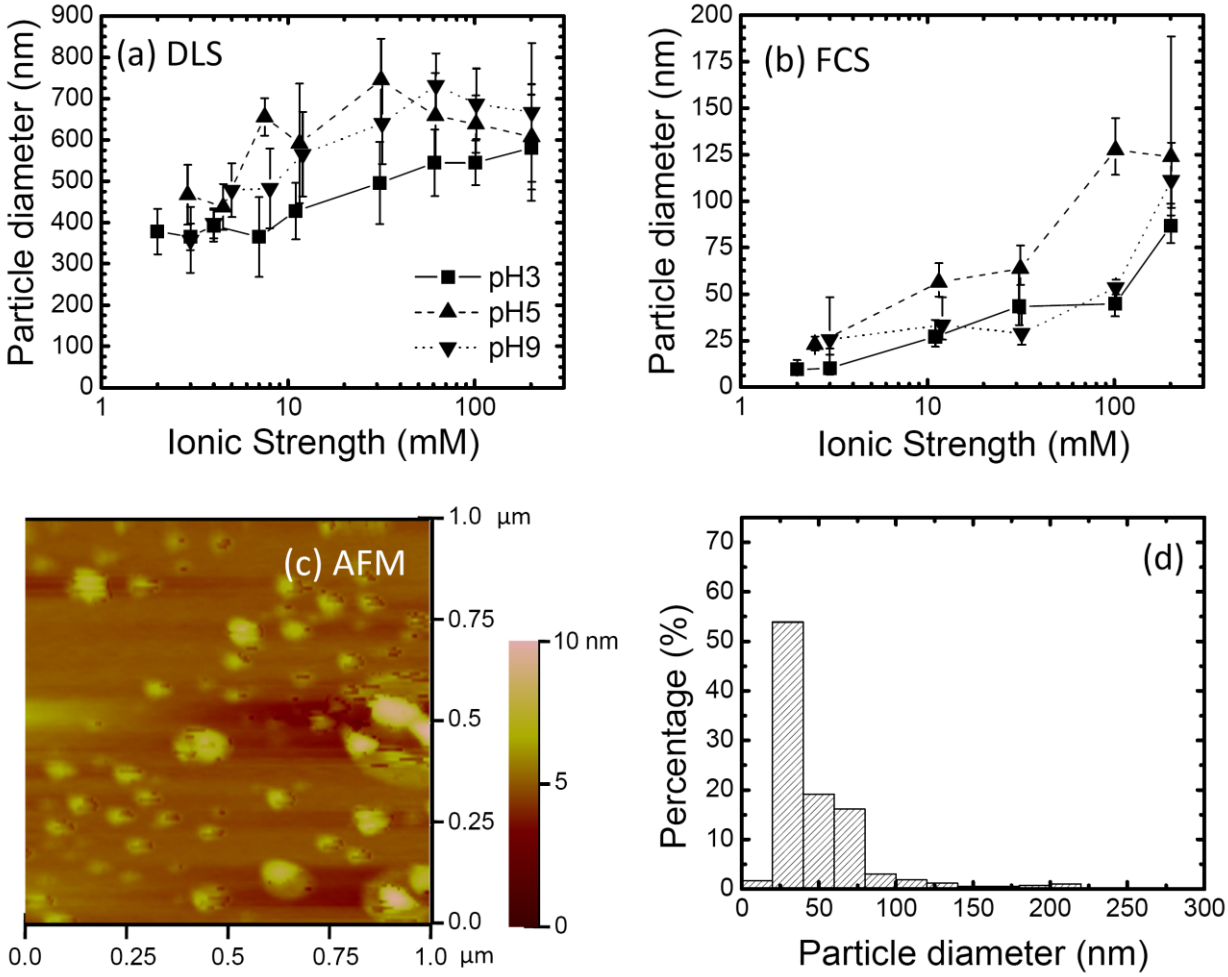

FATISSON et al
FIGURE 1

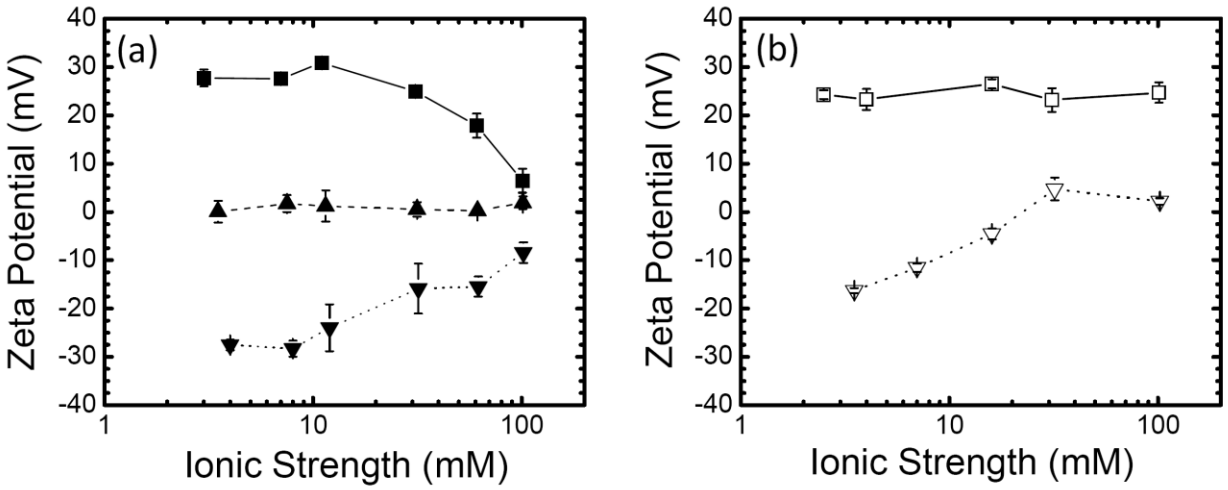

FATISSON et al
FIGURE 2

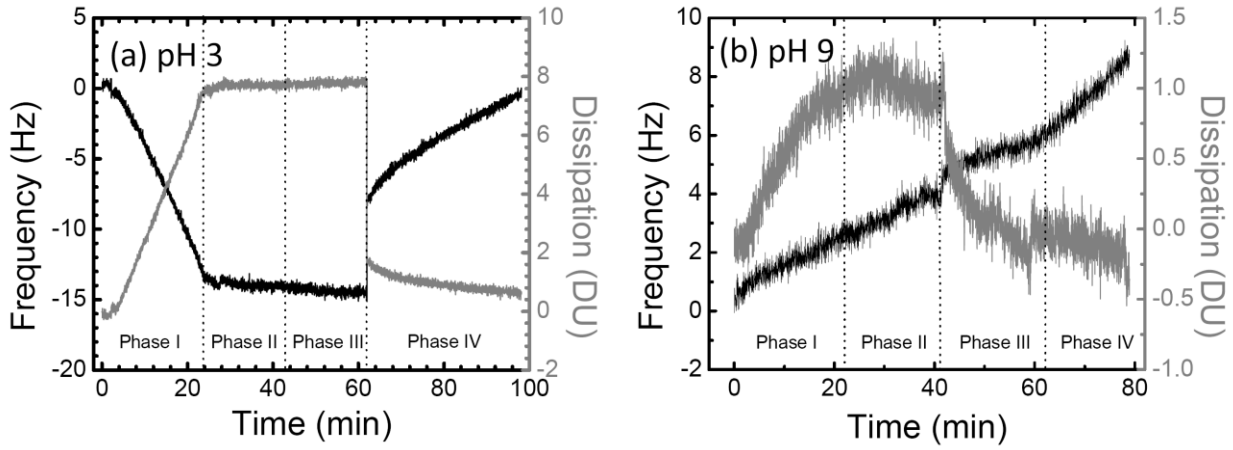

FATISSON et al
FIGURE 3

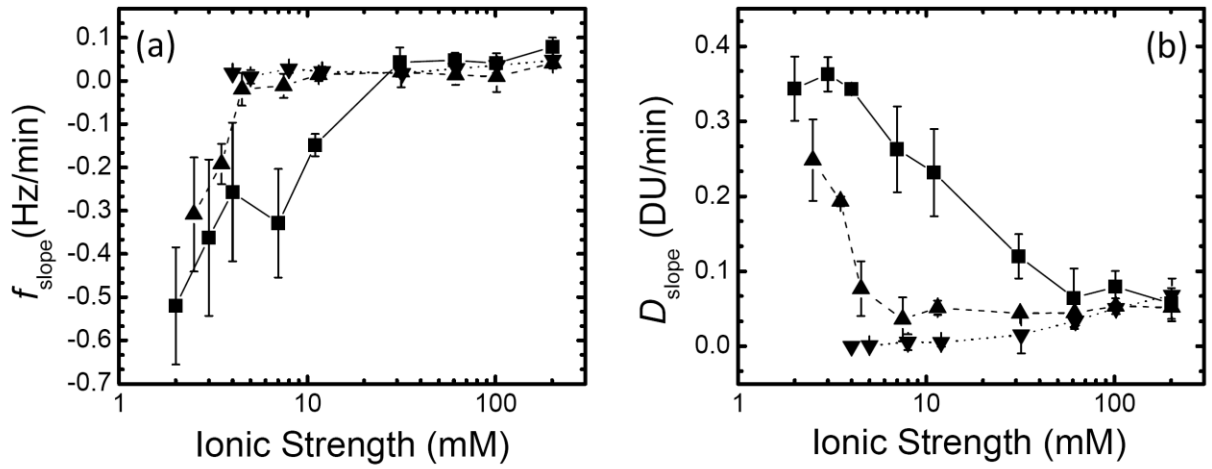

FATISSON et al
FIGURE 4

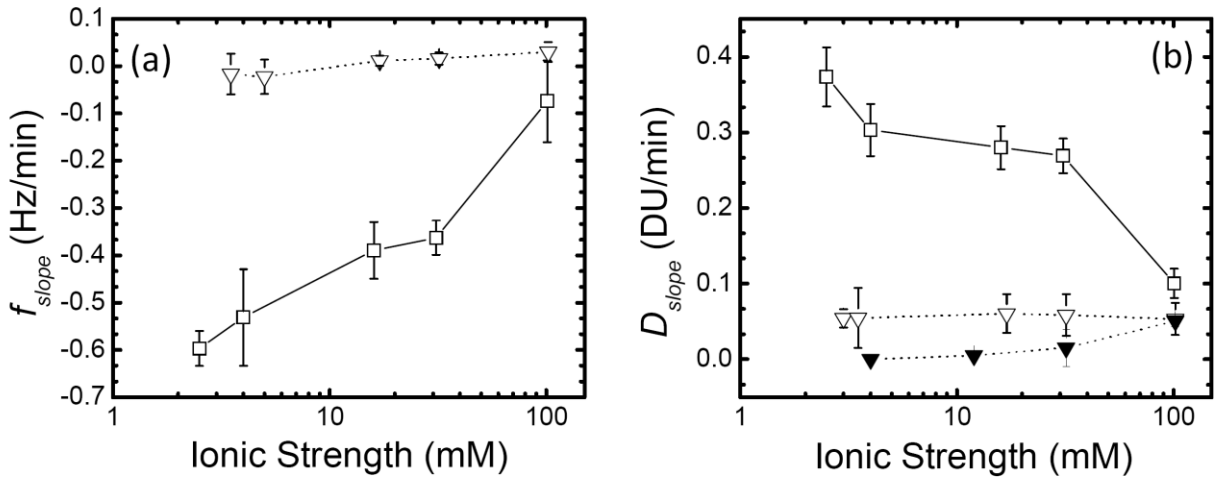

FATISSON et al
FIGURE 5

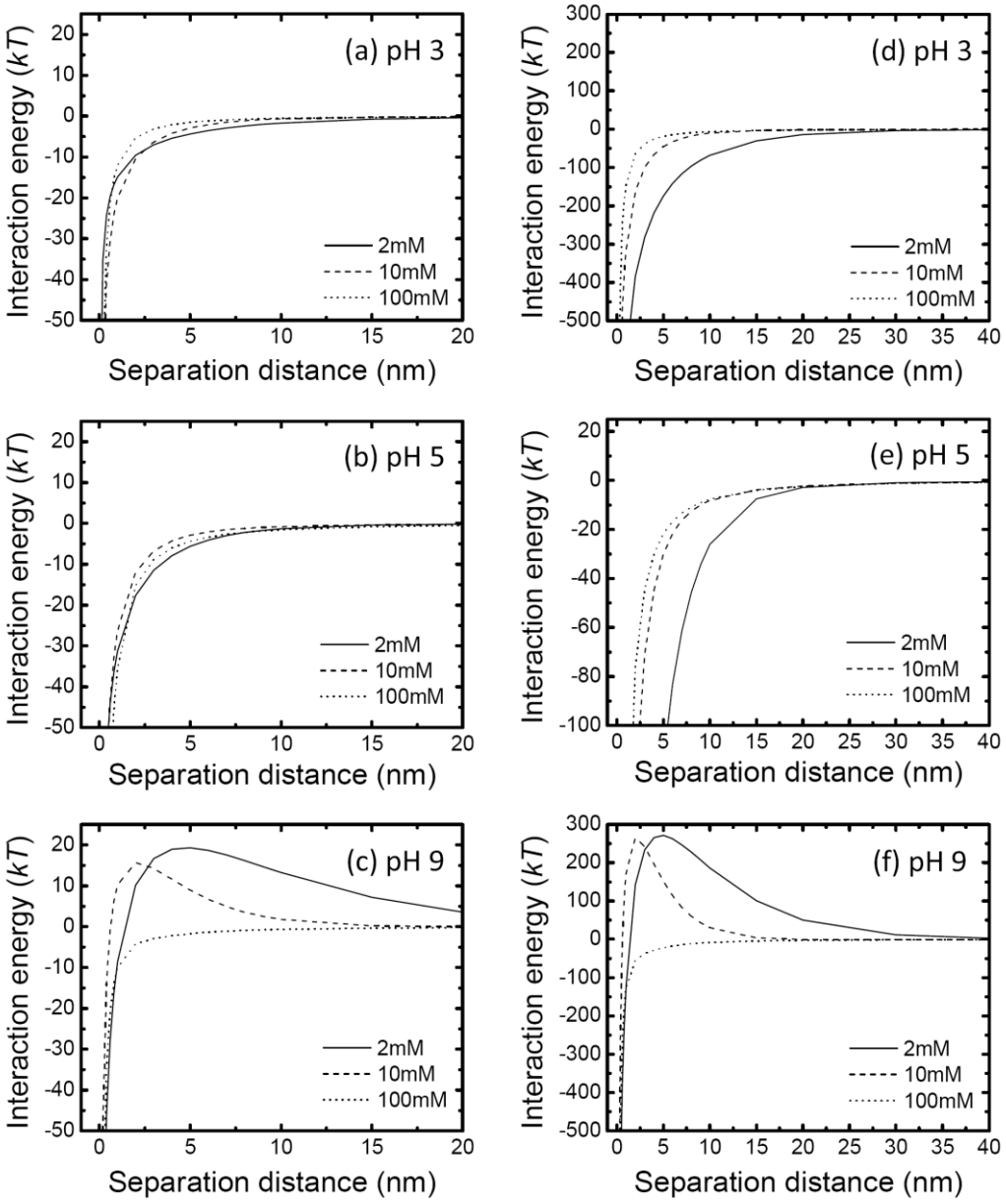

FATISSON et al
FIGURE 6

FOR TABLE OF CONTENTS USE ONLY

TITLE: Deposition of TiO2 Nanoparticles onto Silica Measured Using a Quartz Crystal Microbalance with Dissipation Monitoring

AUTHORS: Julien Fatisson, Rute F. Domingos, Kevin J. Wilkinson and Nathalie Tufenkji